Supplement A Method of analysis

A.1 HL60 cells

In both the HL60 and B16-F1 cells, the width of the lamellipodium is generally small compared to the curvature of the leading edge, which justifies a one-dimensional (1D) analysis. We first determined the cell contour by thresholding the mRFP intensity image, then calculated the normal to this contour at regular spatial intervals. The image was resampled along these normals and the resulting profiles were averaged to give the net 1D distribution, similar to methods described in [1].

For HL60 cells traveling at a velocity v in the negative-x direction, the mRFP intensity distribution $I_R(x,t)$ simply shifts along the x direction, and hence $I_R(x,t) = I_R(x+vt)$ obeys

$$\left(\frac{\partial I_R}{\partial x}\right)_t = -\frac{1}{v}(\omega_- - \omega_+)I_R, \tag{A.1}$$

where the functions $\omega_+(s)$ and $\omega_-(s)$ are the instantaneous rates of monomer association and dissociation in the network frame of reference, which in the most general case are functions of the distance to the leading edge membrane, $s = vt$ (defining $x = 0$ as the location of the leading edge membrane at time $t = 0$). Following the photoactivation of a small rectangular region spanning the width of the lamellipodium, the PA-GFP intensity distribution $I_G(x,t)$, describes the proportion of monomers that have remained incorporated in the network since the moment of photoactivation. Provided that the photoactivated region is small compared to the whole cell volume, changes in $I_G(x,t)$ therefore report on only the dissociation of monomers from filaments in the network as

$$\left(\frac{\partial I_G}{\partial t}\right)_x = -\widetilde{\omega_-} I_G. \tag{A.2}$$

The function $\widetilde{\omega_-}$ is in general a function of both s and t because $I_G(s,t)$ is not a steady-state distribution. Indeed, $\omega_-(s) = \widetilde{\omega_-}(s,t)$ only if all F-actin monomers in the lamellipodium have an equal probability of dissociating at any instant. This equality is guaranteed only immediately after photoactivation at $t = 0$, since at that moment $I_R \propto I_G$ and the initial dissociation of monomers must affect I_R and I_G in equal proportions. Asserting $\widetilde{\omega_-} = \omega_-$ at later times involves a non-trivial assumption of the network structure and detailed biochemical behaviour, which our approach seeks to avoid. However, our experimental results, shown in Sec. 3.2.1 and 3.2.2, are generally consistent with $\widetilde{\omega_-}$ being constant over s and t and equal to ω_-. Equations A.1 and A.2 then combine to give

$$\left(\frac{\partial}{\partial t}\left[\frac{I_G}{I_R}\right]\right)_x = -\omega_+\left(\frac{I_G}{I_R}\right). \tag{A.3}$$

Equations A.2 and A.3 indicate that, in the absence of retrograde flow, as observed for the HL60 cells (see Section 3.1 Results), ω_+ and ω_- may be derived, respectively, from the instantaneous decay rates of I_G/I_R and I_R, measured in the substrate rest frame. [1]

[1] A significant dependence of $\widetilde{\omega_-}$ on location and time since photoactivation would produce noticeable

Provided that $\omega_+$and ω_- are both location-independent (as confirmed to within experimental uncertainty in all the lamellipodia examined, see Section 3.1), Equations A.1-A.3 predict solutions for the HL60 cells of the form

$$I_R(x,t) = I_R^0 \exp[-\kappa(x+vt)] \quad (A.4)$$
$$I_G(x,t) = I_G^0 \exp[-\kappa x - \omega_- t] \quad (A.5)$$

where the spatial decay constant

$$\kappa = (\omega_- - \omega_+)/v \quad (A.6)$$

specifies the length scale of the lamellipodium $L = 1/\kappa$. This exponential dependence is confirmed experimentally in Figure 1d,e.

A.2 B16-F1 cells

In B16-F1 cells, the leading edge is stationary on the substrate and the actin network flows retrogradely, slipping over the substrate at a constant speed v (see Section 3.1). The dynamic behaviour of the B16-F1 cells is formally identical to the HL60 cells, albeit after a change of reference frame $x \to x - vt$. However, performing this transformation would complicate the above analysis (Section A.1) unnecessarily and may introduce systematic errors. A preferable approach is to predict the variations in the fluorescence intensity distributions in the substrate rest frame. The mRFP and PA-GFP decay rates for B16-F1 cells differ from Equations A.1 and A.2 by a convective term that represents the flow of the actin network past the chosen location:

$$(\partial I_R/\partial t)_x = (\omega_+ - \omega_-)\, I_R - v\,(\partial I_R/\partial x)_t = 0 \quad (A.7)$$
$$(\partial I_G/\partial t)_x = -\widetilde{\omega_-} I_G - v\,(\partial I_G/\partial x)_t \quad (A.8)$$

In the steady state, $(\partial I_R/\partial t)_x = 0$ by definition because I_R represents the total F-actin distribution. Therefore, provided that, as with the HL60 cells, ω_+ and ω_- are x-independent and constant over time (a hypothesis we test in Sec. 3.2.2), Equation A.7 yields a general solution

$$I_R(x,t) = I_R^0 \exp(\kappa x) \quad (A.9)$$

with $\kappa = (\omega_- - \omega_+)/v$ as above (Equation A.6). Immediately after photobleaching ($t = 0$), $I_G(x,t)$ must match $I_R(x,t)$ because actin monomers are photoactivated with equal probability. Also, $\widetilde{\omega_-} = \omega_-$ at $t = 0$ because the dissociation of monomers affects I_R and I_G in equal proportions. Therefore, at this instant,

$$\left(\frac{\partial I_G}{\partial t}\right)_x = -(\omega_+ - \omega_- + \widetilde{\omega_-}) I_G = -\omega_+ I_G \quad (A.10)$$

deviations from linearity in the data of Figure 1 and Figure D.1e,h. Equation 3 would then be written as

$$\left(\frac{\partial}{\partial t}\left[\frac{I_G}{I_R}\right]\right)_x = -(\omega_+ - \omega_- + \widetilde{\omega_-})\left(\frac{I_G}{I_R}\right).$$

This was not observed.

Our measurements (linear behaviour on semi-logarithmic axes in Figure D.1h) suggest that Equation A.10 holds, with ω_+ being constant, for a longer time range after photoactivation, implying that $\widetilde{\omega_-} = \omega_-$, and hence that the monomers dissociate from the network with an effectively equal probability, as in the HL60 lamellipodium. Thus, we have the solution

$$I_G(x,t) = I_G^0 \ \exp(-\kappa x - \omega_+ t). \tag{A.11}$$

Because of the added convective contribution, these solutions differ from the HL60 case (Equations A.4, A.5) in two respects: $I_R(x,t)$ has no t dependence and $I_G(x,t)$ here decays with a rate constant ω_+, and not ω_-. For the B16-F1 cells, ω_- is obtained using Equation A.6:

$$\omega_- = \omega_+ + \kappa v.$$

A.3 Cytoplasmic activation of B16-F1 cells

The relevant dynamic equation is adapted from Equation 5 as

$$(\partial I_G/\partial t)_x = \omega_+ I_R(x) - \omega_- I_G - v(\partial I_G/\partial x)_t,$$

where $\omega_+ I_R$ is the rate of fluorescent monomer incorporation, taking $I_\infty(x)$ to be the steady-state distribution approached as $t \to \infty$. The solution

$$I_G(x,t) = I_\infty(x)\left(1 - e^{-\omega_+ t}\right) \tag{A.12}$$

Thus, the constancy of ω_+ and ω_- results in a separation of the spatial and temporal variables.

Supplement B Theoretical model derivation

In a motile (HL60) lamellipodium travelling at speed v in the negative-x direction, the dynamics of one-dimensional F-actin monomer density $A(x,t)$ obeys

$$(\partial A/\partial t)_x = G\delta(x + vt) - (\omega_- - \omega_+)A, \tag{B.1}$$

where $\omega_\pm$ have the same meaning as above and the point-source, of magnitude G, represents the rate of monomer incorporation at the lamellipodium tip, where the free barbed end concentration is highest. This purely formal equation expresses actin dynamics with maximal generality while minimising assumptions on detailed biochemical mechanisms.The constancy of ω_+ and ω_-, observed in our experiments (Sections 3.2.1, 3.2.2), yields the solution

$$A(x,t) = \frac{G}{v} \exp\left[-(\omega_- - \omega_+)t\right] \times H(x + vt)$$

with $H(x)$ the Heaviside function. Consistent with the observed behaviour of $I_R(x,t)$, it represents an exponential function with decay constant $\kappa = (\omega_- - \omega_+)/v$ at a steady speed of v. A corresponding result for stationary (B16-F1) cells is obtained formally by a change of reference frame $x \to x + vt$.

Our central assumption is that ω_+ and ω_- are fully determined by polymerization and depolymerization at barbed and pointed ends, respectively, represented by the distributions $c_{\mathrm{B}}(x,t)$ and $c_{\mathrm{P}}(x,t)$:

$$\text{net local association rate} \equiv \omega_+ A(x,t) = k_+ c_{\mathrm{B}}(x,t) \tag{B.2}$$

$$\text{net local dissociation rate} \equiv \omega_- A(x,t) = k_- c_{\mathrm{P}}(x,t). \tag{B.3}$$

Each polymerization (depolymerization) reaction advances the barbed (pointed) end forward by a length increment a that accounts for both the size of an individual actin monomer and the orientation of the filament relative to the direction of motion. Thus, whereas individual actin monomers in the HL60 network are immobile relative to the substrate, the barbed ends (and the lamellipodium tip) are all assumed to advance at a speed

$$v = ak_+. \tag{B.4}$$

and pointed ends at a speed ak_-, both in the direction of the cell motion. Other biochemical processes are assumed to contribute to the dynamics only via their effect on $c_{\mathrm{B}}(x,t)$ and $c_{\mathrm{P}}(x,t)$. The processes included in the model are listed in Table 1. The formulation of the rate of each process, given in the rightmost column, generally assumes that processes occur with an effectively equal probability anywhere in the network, regardless of the location along the filaments.

Barbed-end capping diminishes the free barbed-end concentration c_{B} and augments the capped barbed-end concentration c_{C} at a rate given by k_{c}. A severing event (k_{s}) produces simultaneously a free barbed and a free pointed end. Likewise, side branching (k_{B}) creates one free barbed end together with a capped pointed end (filament-junction concentration c_{J}). Based on experimental evidence [2], we assumed that barbed-end uncapping does not occur until complete depolymerisation of filaments. To avoid speculative assumptions on the filament length distribution within the lamellipodium, we resort to a statistical argument to estimate the frequency of complete filament depolymerisation. Taking c_{C}/A as the proportion of depolymerization reactions occuring in filaments with a capped barbed-end, we estimate the frequency of simultaneously removing a free pointed-end and a capped barbed-end as $k_- c_{\mathrm{P}} c_{\mathrm{C}}/A$. A capped pointed end is then "freed" from a junction either by spontaneous unbranching (rate k_{U}) or when the pointed end of the mother filament catches up with the junction. Following a similar reasoning to the one above, we estimate the rate at which a depolymerising pointed end coincides with a junction as $k_- c_{\mathrm{P}} c_{\mathrm{J}}/A$, where c_{J}/A is the estimated proportion of actin monomers located at a junction.

These processes define the contributions to the time derivatives of each distribution, written in the formalism of Mogilner et al. [3] and Dawes et al. [4], which yield steady-state travelling-wave solutions for the actin density along the x-direction (i.e. a motile lamellipodium that preserves a constant width). Combining the empirical Equation B.1 with Equations B.2 and B.3 yields:

$$\partial A/\partial t = k_+ c_{\mathrm{B}} - k_- c_{\mathrm{P}} \tag{B.5}$$

Table 1: Kinetic formulation of network regulatory processes used in the theoretical model, expressed in terms of concentrations of F-actin (A), free barbed ends (c_{B}), free pointed ends (c_{P}), capped barbed ends (c_{C}) and capped pointed ends (c_{J}). A '+' represents the generation of a new filament end, and '-' its removal by a given process.

Event	$\mathbf{c_B}$	$\mathbf{c_P}$	$\mathbf{c_C}$	$\mathbf{c_J}$	**kinetic expression**
severing	+	+			$k_{\mathrm{s}}A$
side branching	+			+	$k_{\mathrm{B}}A$
pointed meets barbed end		-	-		$k_{-}\frac{c_{\mathrm{C}}c_{\mathrm{P}}}{A}$
barbed-end capping	-		+		$k_{\mathrm{c}}c_{\mathrm{B}}$
pointed-end uncapping		+		-	$k_{\mathrm{U}}c_{\mathrm{J}}$
pointed end meets filament junction		+		-	$k_{-}\frac{c_{\mathrm{P}}c_{\mathrm{J}}}{A}$

with

$$\begin{aligned}
\partial c_{\mathrm{B}}/\partial t &= -ak_{+}(\partial c_{\mathrm{B}}/\partial x) - k_{\mathrm{c}}c_{\mathrm{B}} + k_{\mathrm{s}}A + k_{\mathrm{B}}A \\
\partial c_{\mathrm{P}}/\partial t &= -ak_{-}(\partial c_{\mathrm{P}}/\partial x) + k_{\mathrm{s}}A - k_{-}(c_{\mathrm{P}}c_{\mathrm{C}}/A) + k_{-}(c_{\mathrm{P}}c_{\mathrm{J}}/A) + k_{\mathrm{U}}c_{\mathrm{J}} \\
\partial c_{\mathrm{C}}/\partial t &= k_{\mathrm{c}}c_{\mathrm{B}} - k_{-}(c_{\mathrm{P}}c_{\mathrm{C}}/A) \\
\partial c_{\mathrm{J}}/\partial t &= -k_{-}(c_{\mathrm{P}}c_{\mathrm{J}}/A) + k_{\mathrm{B}}A - k_{\mathrm{U}}c_{\mathrm{J}}
\end{aligned}$$

This equation system naturally reproduces Equation 1, the empirical representation of the experimental results of Figures 1, 2, and 3. It is straightforward to show that the solutions for the distributions A, c_{B}, c_{P}, c_{C}, and c_{J} all display the same exponential dependence $\sim \exp[\kappa(x - vt)]$ all characterised by a unique spatial decay constant κ, consistent with the experimental finding that κ is characteristic of F-actin, ARPC4, barbed-ends, and pointed-ends in the lamellipodium.

The differential equation system was solved analytically (Matlab Symbolic Math Toolbox, The Mathworks, Inc., Natick, Massachusetts, USA) to give the distribution amplitudes, expressed in function of the amplitude of the distribution A :

$$c_{\mathrm{B}} = \frac{k_{\mathrm{s}} + k_{\mathrm{B}}}{k_{\mathrm{c}}} \times A \tag{B.6}$$

$$c_{\mathrm{P}} = \frac{k_{\mathrm{c}}(k_{+}k_{\mathrm{s}} + k_{\mathrm{c}}k_{\mathrm{U}})}{(k_{+} - k_{-})\left[k_{+}\left(k_{\mathrm{s}} + k_{\mathrm{B}}\right) + k_{\mathrm{c}}k_{\mathrm{U}}\right]} \times A \tag{B.7}$$

$$c_{\mathrm{C}} = \frac{k_{\mathrm{c}}}{k_{+}} \times A \tag{B.8}$$

$$c_{\mathrm{J}} = \frac{k_{\mathrm{B}}k_{\mathrm{c}}}{k_{+}(k_{\mathrm{s}} + k_{\mathrm{B}})} \times A \tag{B.9}$$

and

$$\kappa = \left[\underbrace{\frac{k_{\mathrm{c}}k_{-}}{k_{+}(k_{+} - k_{-})} \cdot \frac{k_{+}k_{\mathrm{s}} + k_{\mathrm{c}}k_{\mathrm{U}}}{k_{+}(k_{\mathrm{s}} + k_{\mathrm{B}}) + k_{\mathrm{c}}k_{\mathrm{U}}}}_{=\left(\frac{k_{-}}{k_{+}}\right)c_{\mathrm{P}}/A} - \underbrace{\frac{k_{\mathrm{s}} + k_{\mathrm{B}}}{k_{\mathrm{c}}}}_{=c_{\mathrm{B}}/A} \right] \frac{1}{a}. \tag{B.10}$$

Equation B.10 represents a useful model output because $1/\kappa$ is the directly measurable length scale of the lamellipodium: the greater the spatial decay constant κ, the narrower the lamellipodium. The amplitudes of the c_{B}, c_{P}, c_{C}, and c_{J} distributions are more challenging to measure, requiring the selective labelling and precise quantification of free barbed-ends, free pointed-ends, capped barbed-ends, and capped pointed-ends. A physical interpretation of Equation B.10 is obtained by comparison with Equations B.4, B.6 , and B.7:

$$\kappa v = \left(k_{-}c_{\mathrm{P}} - k_{+}c_{\mathrm{B}}\right)/A \tag{B.11}$$

This equation is essentially a restatement of $\kappa = (\omega_{-} - \omega_{+})/v$ (Equation 4) in terms of the polymerization and depolymerization rates. A phenomenological interpretation of this result is that the average rate of turnover, measured by κv, is controlled by the difference between the rates of monomer release ($k_{-}c_{\mathrm{P}}$) and incorporation ($k_{+}c_{\mathrm{B}}$). In other words, κv is given by the balance between k_{+} and k_{-}, weighted by c_{B} and c_{P}, respectively. Equation B.4 expressed v directly in terms of the *absolute* value of k_{+}, independently of k_{-}, because it is the incorporation of monomers at the tip of the lamellipodium that advances the leading edge by one monomer length. The interplay of k_{+} and k_{-} in κ is more complex. Equation B.10 predicts that κ is approximately a linear function of $(k_{-}/k_{+})/(k_{+} - k_{-})$, a parameter more sensitive to the *difference* between k_{+} and k_{-}, in both absolute and relative terms. This reasoning applies equally to the HL60 and B16-F1 cells, since our results suggest that the qualitative dynamics of both cell types are made formally equivalent by a change of reference frame ($x \to x + vt$).

Equations B.6-B.10 allow prediction of the kinetic dependences of the steady-state lamellipodium characteristics κ and v. However, without systematically calibrating fluorescence intensities for A, c_{B}, c_{P}, c_{C}, and c_{J}, these predictions only indicate qualitative trends. Nonetheless, these qualitative predictions can be tested by altering kinetic parameters by genetic or pharmacological perturbation. The resulting trends for perturbation of each parameter are summarized in the table in Figure 7.

Supplement C Protocols

C.1 Cell lines

C.1.1 HL60 cell culture and under-agarose motility assay

The neutrophil-like human promyelocytic leukaemia cell line HL-60 was a kind gift of Dr Orion Weiner (University of California in San Francisco). Cells were maintained in RPMI 1640 with Glutamax (Invitrogen), 10% fetal bovine serum, and penicillin/streptomycin (P/S). Cells were passaged every 3-4 days to maintain cell concentration between 10^5 and 10^6 cells/mL. Cells were differentiated by addition of 1.3% DMSO to the culture medium and left to differentiate for 3-5 days. On the day of the experiment, cells were resuspended in Hank's Buffered Saline Solution (HBSS) supplemented with 1% Human Serum Albumin (HSA).

We observed chemotaxis of differentiated HL60 cells in response to fMLP chemoattractant in "under agarose" assays [5], which favour the formation of broad easily observable

lamellipodia while preventing ruffling. Agarose gels with thicknesses of $\sim$ 3mm were cast into 35-mm-diameter glass-bottomed petri dishes as described by Heit and Kubes [6]. Two wells (diameter $\sim$ 4 mm, separated by $\sim$ 1 cm were made with a biopsy punch. Each well was filled with 25 μl of HBSS/HSA containing $\approx 10^4$ differentiated HL-60 cells and 100 nM of fMLP chemoattractant, respectively. Observations were carried out after 1h incubation at 37°C.

C.1.2 B16-F1 cell culture and lamellipodial induction

Mouse melanoma cells (B16-F1) were cultured at 37°C in a 5% CO_2 atmosphere in high-glucose (4.5 g/l) Dulbecco's modified Eagle's medium (Sigma-Aldrich) supplemented with 10% FBS and P/S. Prior to experimentation, cells were detached from culture flasks using trypsin-EDTA and resuspended in Leibovitz buffer L15 containing 10% FBS. Cells were then plated onto fibronectin coated acid-washed coverslips. Briefly, glass coverslips (25 mm diameter) were flamed, acid-washed by incubation in 1 M HCl at 60°C for 6 hours, sonicated in water for 30 min, and in 95% ethanol for 30 min. On the day of the experiment, they were coated with 50 μg/ml fibronectin in PBS for 1 hour at 37°C. 200 μl of the cell suspension ($\approx$ 5000 cells) was applied to the coverslips and cells were left to adhere for at least 30 min at 37°C. Lamellipodia were induced by addition of aluminofluoride solution to the medium (final concentrations 50 μM $AlCl_3$ and 30 μM NaF [7]) followed by incubation at 37°C for 15 min.

C.1.3 Generation and maintenance of stable cell lines

To examine localisation of cytoskeletal proteins in the lamellipodium, we generated HL60 and B16-F1 cell lines stably expressing proteins tagged with fluorescent proteins (FP). Creation of all lines followed the same procedure: cDNA encoding the protein of interest tagged with FP was excised from a donor vector and inserted into the retroviral vectora pRetro-QAcGFPC1 or pLNCX2 (Takara-Clontech). Actin-mRFP-PA-GFP was previously described [8]. P20/ARPC4 was a kind gift of Prof Klemens Rottner (University of Bonn). Retroviruses were then generated by transfecting the plasmids into 293-GPG cells for packaging (a kind gift from Prof Daniel Ory, Washington University, USA. Retroviral supernatants were then harvested and used to transduce wild type cells. For transduction with retrovirus, 5×10^4 cells were centrifuged at 1500 RPM for 3 minutes and resuspended in 1 ml of viral supernatant with 8 μl/ml polybrene. The resulting suspension was incubated at 37°C for 5-6 hours before a second round of transduction. After 2-3 day recovery, cells were selected with the appropriate antibiotic (1 μg/ml of puromycin or 1 mg/ml G418).

C.2 Verification of the steady state

To confirm the existence of steady state, we first used photobleaching and photoactivation to determine the actin turnover time (defined as giving at least 90% fluorescence recovery): 56 ± 17 s for B16-F1 cells and 31 ± 5 s for HL-60 cells (N=8 cells and 7 cells, respectively, illustrated in Figures 1 and 2). These measurements enabled us to determine the time scale over which cell shape and intensity distributions needed to remain constant for the cells to

be considered at steady state. Over time scales of order 1 minute, we found the mRFP fluorescence intensity distribution to be well described by a decaying exponential function (see Figures 1, 2, and D.1), as previously reported for fish keratocytes [9]. When the spatial decay constant κ remained constant to within 5% over the observation period, we concluded that the cell was at steady state.

C.3 Imaging and photoactivation measurements

Imaging and photoactivation were done on an Olympus FV-1000 scanning laser confocal microscope interfaced to an IX-81 inverted microscope using a 100× oil-immersion objective (UPlanSApo, NA = 1.4, Olympus). Individual cells with a well developed and uniform lamellipodium were first identified from the mRFP fluorescence signal by epi-illumination. Cells were considered suitable for analysis if they displayed a regular lamellipodium over a contour distance at least five times longer than the lamellipodium width. This criterion facilitated the confirmation that the lamellipodia remained in a steady state and that measurements were not contaminated by extraneous actin structures. It also allowed the removal of irregularities in the B16-F1 cells by spatial averaging, as described below.

In HL60 cells, a rectangular region of interest was then chosen with its long axis perpendicular to the leading edge membrane with a length of $2 - 5$ μm and a width of ~ 1 μm to photoactivate the lamellipodium over its entire cross section. Averaging across the photoactivation region ensured that local inhomogeneities in lamellipodial structure did not affect measurements. Exposure times to 405 nm light were determined empirically and the laser power was sufficiently weak that the overall behavior and the non-exposed regions were unaffected by photoactivation. Images in the mRFP and PA-GFP channels were then captured continuously in the region of interest until the PA-GFP fluorescence signal had completely decayed, a duration corresponding to the lamellipodium turnover time. Cells for which the mRFP fluorescence intensity distribution changed noticeably on a time-scale comparable to turnover time were considered not to be in steady-state and were discarded. The mRFP and PA-GFP intensities were then averaged across the width of the region of interest to yield the spatial intensity profile across the lamellipodium cross section.

C.4 Image analysis

All image analysis was performed in Matlab (The Mathworks, Natick, Massachusetts). Images were low-pass-filtered (with a 3-pixel window) to give an effective resolution of 0.2 μm. The cell contour was then determined using a custom-built edge-detection algorithm applied to the mRFP-actin distribution (for live cells) or rhodamine-phalloidin fluorescence image (for fixed cells, see Section C.5). One-dimensional actin distributions were generated by first calculating the vector normal to the contour at pixel-size distance intervals, and then sampling the intensity images along this vector, again at pixel-size intervals. The intensity signal at each distance x from the leading edge membrane was then averaged over the whole width of this effectively "straightened" lamellipodium.

C.5 Tropomodulin and F-actin localisation

To determine the free pointed-end distribution in the lamellipodium, we employed the protocol detailled by Miyoshi et al. [10]. Briefly, GST tagged GFP-tropomodulin (a kind gift from Prof N Watanabe, Tohoku University) was expressed in BL21 pLysS cells and purified with standard methods for GST tagged protein purification. For labelling pointed-ends, B16-F1 cells plated onto glass coverslips were permeabilised for 30 s in cytoskeleton buffer (10 mM MES, 90 mM KCl, 3 mM $MgCl_2$, 2 mM EGTA, 160 mM sucrose, pH 6.8) containing 1% TritonX-100 and 200 μg/ml tropomodulin-GFP. The cells were then rinsed gently in intracellular buffer (IB) (10 mM HEPES, 100 mM KCl, 2 mM $MgCl_2$, 0.2 mM EGTA, 1 mM DTT, pH 6.8), fixed in a 2.5% glutaraldehyde solution in IB for 10 min, incubated 5 min in IB containing 10 mg/ml bovine serum albumin (BSA), and 15 min in IB-BSA with 5 μg/ml rhodamine-phalloidin. Images were then captured on a spinning disk confocal (CSU-22, Hamamatsu) equipped with an Andor iXon camera (Andor, Belfast, UK).

C.6 CK666 perturbation

CK666 was purchased from Merck Biosciences and used to perturb Arp2/3 complex mediated actin nucleation. Chemical perturbation experiments were carried out as follows. The cell was first examined for at least 5 minutes to ensure that it was at steady state. The concentration of CK666 was then increased from zero in increments of 5 or 10 μM, and the cell was left to reach steady state. We assumed steady state if cells maintained a constant lamellipodium width over 5 minutes.

Supplement D Supplementary results for B16-F1 cells

References

[1] Ponti, A., 2004. Two Distinct Actin Networks Drive the Protrusion of Migrating Cells. *Science* 305:1782–1786.

[2] Lai, F. P., M. Szczodrak, J. Block, J. Faix, D. Breitsprecher, H. G. Mannherz, T. Stradal, G. A. Dunn, J. V. Small, and K. Rottner, 2008. Arp2/3 complex interactions and actin network turnover in lamellipodia. *EMBO Journal* 27:982–992.

[3] Mogilner, A., and L. Edelstein-Keshet, 2002. Regulation of actin dynamics in rapidly moving cells: a quantitative analysis. *Biophysical Journal* 83:1237–1258.

[4] Dawes, A. T., G. Bard Ermentrout, E. Cytrynbaum, and L. Edelstein-Keshet, 2006. Actin filament branching and protrusion velocity in a simple 1D model of a motile cell. *Journal of Theoretical Biology* 242:265–279.

[5] Nelson, R., P. Quie, and R. L. Simmons, 1975. Chemotaxis under agarose: a new and simple method for measuring chemotaxis and spontaneous migration of human polymorphonuclear leukocytes and monocytes .

[6] Heit, B., and P. Kubes, 2003. Measuring Chemotaxis and Chemokinesis: The Under-Agarose Cell Migration Assay. *Science Signaling* 2003:pl5.

[7] Hahne, P., A. Sechi, and S. Benesch, 2001. Scar/WAVE is localised at the tips of protruding lamellipodia in living cells. *FEBS letters* .

[8] Kueh, H. Y., G. T. Charras, T. J. Mitchison, and W. M. Brieher, 2008. Actin disassembly by cofilin, coronin, and Aip1 occurs in bursts and is inhibited by barbed-end cappers. *Journal of Cell Biology* 182:341–353.

[9] Ofer, N., A. Mogilner, and K. Keren, 2011. Actin disassembly clock determines shape and speed of lamellipodial fragments .

[10] Miyoshi, T., T. Tsuji, and C. Higashida, 2006. Actin turnover–dependent fast dissociation of capping protein in the dendritic nucleation actin network: evidence of frequent filament severing. *Journal of Cell Biology* 175:947–955.

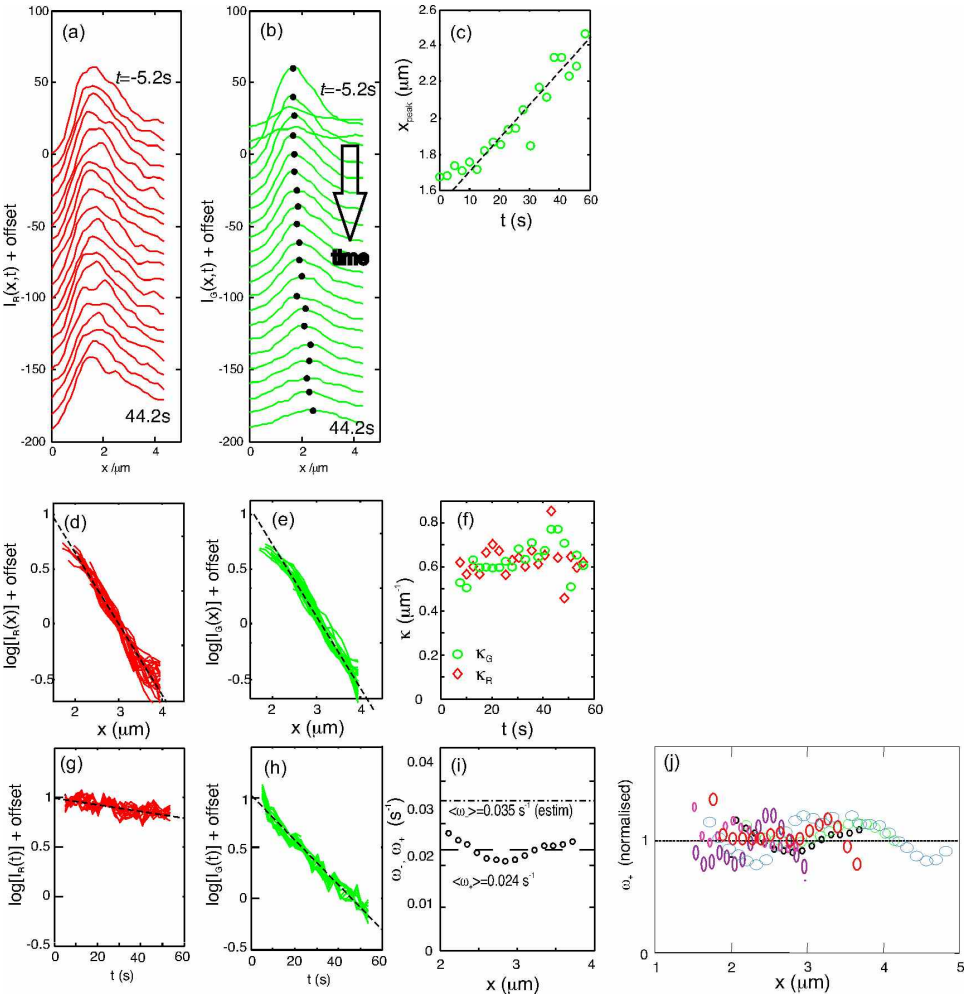

Figure D.1: Photoactivation of the rectangular region of a B16-F1 cell shown in Figure 2. (a) The mRFP (I_R) and (b) the PA-GFP (I_G) fluorescence intensity distributions plotted as functions of x, at regular time intervals of 2.6 s after photoactivation. I_R remains stationary throughout the recovery, but the peak in I_G moves to the right with average velocity $v = 1.0$ μm/min. (c) The peak displacement in I_G as a function of time, with average gradient v. (d, e) The I_R and I_G data of (a) and (b), respectively, are normalised to their values at $x = 0$ for each t, and plotted on logarithmic axes to confirm the exponential decay and the similarity of the gradients at every time point. (f) The gradients in (d) and (e) yield the spatial decay constants κ of the PA-GFP intensity distribution $I_G(x,t)$ (green circles, mean value $\langle\kappa\rangle = 0.63 \pm 0.06$ μm^{-1}) and of the mRFP distribution $I_R(x,t)$ (red diamonds, $\langle\kappa\rangle 0.66 \pm 0.03$ μm^{-1}), as functions of time. There is no significant time dependence in either case. (g, h) The same data I_R and I_G are normalised to their value at $t = 0$ and plotted on logarithmic axes as functions of time. The straight lines, for different values of x, are again consistent with an exponential decay with time. (i) The slopes of the curves in g and h give the temporal decay constant ω_+ for each location x (see Equation A.10), with a mean value $\langle\omega_+\rangle = 0.024 \pm 0.002$ s^{-1} and show little x dependence. The dash-dot line indicates the expected $\langle\omega_-\rangle \equiv \langle\omega_+\rangle + \kappa v \approx 0.035$ s^{-1} (Equation 4). (j) The analysis of (i) was repeated in 6 cells. Values of ω_+ (normalised to their mean value) versus x are plotted for six different cells and show no systematic trend.

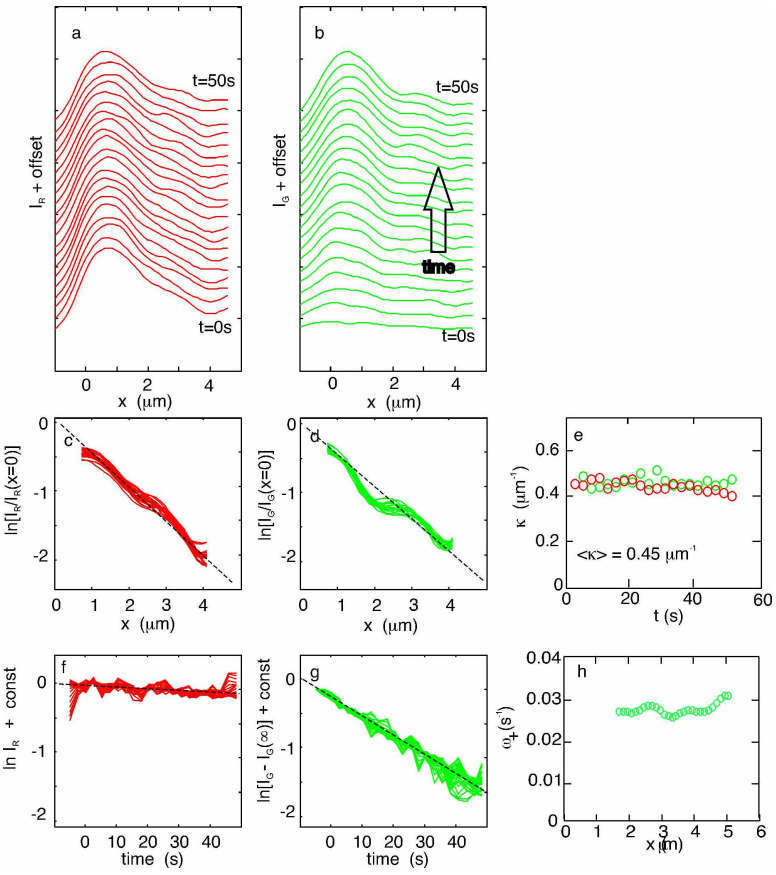

Figure D.2: Cytoplasmic activation of a B16-F1 lamellipodium (see Section 3.2.3 and Figure 3). (a) mRFP (I_R) and (b) PA-GFP (I_G) intensity distributions are plotted as functions of x in time intervals of 2.5 s. (c, d) The logarithm of the data points in (a) and (b), at x values greater than the intensity maximum, are normalised to their values at $x = 0$. The linear relationships confirm exponential decay for both channels. (e) The spatial decay constants, given by the gradient of the data in c (red symbols) and d (green symbols), are plotted as functions of time and show good agreement between I_R and I_G and little variation over the F-actin turnover time. Average $\langle\kappa\rangle = 0.49\ \mu\text{m}^{-1}$. (f) The mRFP data normalised to their value at $t = 0$ and plotted as a function of time. Each curve represents a different x value and shows minimal decay of I_R with time for all x. (g) The I_G data in (b) display a temporal recovery of the form $y(t) = y_\infty(1 - e^{-bt})$, as shown in Figure 3d). Here, we plot $\ln(y(t) - y_\infty) + \text{constant}$ to show that the approach to the asymptotic limit y_∞ is exponential. (h) The gradients of the lines in g show no x dependence and are associated with the effective rate constant ω_+ (see Section A.3).